Limited local electron-lattice coupling in manganites: An electron diffraction study

D. Sánchez,[1] M. J. Calderón,[2] J. Sánchez-Benítez,[3] A. J. Williams,[3] J. P. Attfield,[3] P. A. Midgley,[1] and N. D. Mathur[1,*]

[1]*Department of Materials Science, University of Cambridge, Pembroke Street, Cambridge CB2 3QZ, United Kingdom*

[2]*Instituto de Ciencia de Materiales de Madrid (CSIC), Cantoblanco, 28049 Madrid, Spain*

[3]*School of Chemistry and Centre for Science at Extreme Conditions, University of Edinburgh, West Mains Road,*
Edinburgh EH9 3JJ, United Kingdom

$(Pr,Ca)MnO_3$ is the archetypal charge-ordered manganite, but in $Pr_{0.48}Ca_{0.52}MnO_3$, we find (using convergent-beam electron diffraction and dark-field images) that the superlattice period is locally incommensurate with respect to the parent lattice and that the superlattice orientation possesses significant local variations. This suggests that local electron-lattice coupling never overwhelmingly dominates the rich physics of manganites, even in the most extreme scenarios that produce the largest colossal magnetoresistance effects.

PACS number(s): 75.47.Lx, 71.38.−k, 71.45.Lr

In chemically single-phase perovskite manganites, there is widespread interest in the coexistence of magnetic and electronic phases over a wide range of length scales.[1,2] One of the predominant phases possesses a superlattice (below T_s) that is traditionally associated with charge order[3,4] (CO) arising due to strong local electron-lattice (Jahn-Teller) coupling.[5] The concept of strong coupling is entrenched in manganite physics because it is also considered[1] necessary for colossal magnetoresistance[6,7] (CMR) and the pronounced influence of strain on physical properties.[8] Here, we investigate a member of the $(Pr,Ca)MnO_3$ family that epitomises[1,7,9–12] strong coupling. Surprisingly, we find that the local coupling is too weak to force the superlattice to be (i) locally commensurate or (ii) aligned with the parent lattice. This suggests that local coupling is of limited strength, thus extending the validity of a recent mean-field reinterpretation[13] cast purely in terms of magnetization and charge density.

In manganite compositions that show ferromagnetic metallic (FMM) phases, the electron-lattice coupling is limited.[1] At low temperatures, the effective coupling is reduced by metallic screening, and even in the vicinity of the Curie temperature, the high-field magnetoresistance effects are not colossal (e.g., just 4% at 5 T in[14] $La_{0.7}Sr_{0.3}MnO_3$ and 900% at 4 T in[15] $La_{0.75}Ca_{0.25}MnO_3$). The discovery[6] of CMR (10^6% in 6 T) was made in a similar composition ($La_{0.67}Ca_{0.33}MnO_3$), but only in a sample where the microstructure had been altered by thin-film strain and annealing.

The largest CMR effects[7] (10^{10}% at 5 T for $Pr_{0.67}Ca_{0.33}MnO_3$) in manganites arise at low temperatures in phases where it is believed[1] that strong electron-lattice coupling produces charge order. This phase is characterized by a superlattice (wave vector $\mathbf{q} \| \mathbf{a}^*$) seen in electron,[3,4] x-ray,[16] and neutron[16,17] diffraction experiments. Originally, this was interpreted[3,4] in terms of (200) planes containing the idealized cation Mn^{4+}, interspersed with orbitally ordered Mn^{3+} planes (indexing the room temperature cell as orthorhombic *Pnma*). However, the key electron microscopy evidence for this description was overinterpreted and the nature of the modulations remains controversial.[18]

Recently, we argued[18,19] against strong electron-lattice coupling in the modulated (so-called CO) phases of $(La,Ca)MnO_3$. Subsequently, our experimental findings were found to be reasonable in theoretical models where modulated phases are stabilized with small and even zero electron-lattice coupling.[13,20] However, one anticipates that our evidence[18,19] against strong coupling in $(La,Ca)MnO_3$ would not extend to a supposedly strong[1,7,9–12] CO manganite such as $(Pr,Ca)MnO_3$. However surprisingly, in $Pr_{0.48}Ca_{0.52}MnO_3$, we find two independent pieces of evidence against strong local coupling. First, convergent-beam electron diffraction (CBED) data for $Pr_{0.48}Ca_{0.52}MnO_3$ show that the superlattice is incommensurate with the parent lattice (cf. our $La_{0.48}Ca_{0.52}MnO_3$ data).[18] Second, we reveal that the superlattice orientation varies (i) locally in dark-field images as with $(La,Ca)MnO_3$ (Ref. 21) and (ii) on a 100 nm length scale, where pronounced misorientations of $\mathbf{q}$ with respect to $\mathbf{a}^*$ are seen below 150 K, which we identify as the Néel temperature[9,17] T_N ($<T_s$).

Polycrystalline $Pr_{0.48}Ca_{0.52}MnO_3$ with micron-sized grains was prepared by repeated grinding, pressing, and sintering of stoichiometric Pr_6O_{11}, $CaCO_3$, and MnO_2. Initially, it was heated at 950 °C for 12 h to decarboxylate the $CaCO_3$, and then it was twice reground, repelleted, and heated at 1350 °C for 4 days. X-ray powder diffraction in a Philips PW1050 diffractometer (Cu $K\alpha$) recorded only a single phase, and we infer that at least the grains of interest are chemically homogeneous given that we observe q/a^* to be highly homogeneous. Electrically, the sample was found to be insulating and our resistance measurements suggest that 230 K$<T_s$ $<$250 K as expected.[22] Electron transparency was achieved by conventional mechanical polishing and argon-ion thinning. A Philips CM30 transmission electron microscope was used to collect CBED patterns and 500 nm selected-area diffraction (SAD) patterns. The microscope is equipped with a Gatan double-tilt liquid nitrogen (LN$_2$) stage with an effective base temperature of ∼120 K. A Philips CM300 field emission gun transmission electron microscope, equipped with a Gatan image filter and charge-coupled device camera, was used to collect energy-filtered 100 nm SAD patterns and dark-field images. This microscope supports Gatan sample stages with base temperatures of ∼9.6 K (helium, data on warming only) and ∼90 K (nitrogen).

Figure 1 repeats for $Pr_{0.48}Ca_{0.52}MnO_3$ the key CBED evidence[18] in $La_{0.48}Ca_{0.52}MnO_3$ which shows that the superlattice is locally incommensurate with a highly uniform pe-
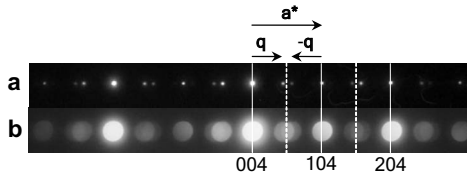
FIG. 1. Electron diffraction patterns for a $Pr_{0.48}Ca_{0.52}MnO_3$ grain near 120 K. Solid lines indicate parent reflections separated by reciprocal lattice vector **a***. The superlattice (wave vector **q**) produces reflections at (a) q/a^*=0.4379(3) in a 500 nm selected-area diffraction (SAD) pattern and (b) q/a^*=0.440(1) in a convergent-beam electron diffraction (CBED) pattern (spot size of $\sim$3.6 nm). The dramatic reduction in the experimental length scale from (a) to (b) yields in effect no change in q/a^* [the 0.5% difference falls within the small observed intragranular variation (Ref. 18) in q]. In particular, a lock-in to q/a^*=0.5 (dashed lines) was not seen in all CBED patterns from this and other grains (with one exception that is irrelevant because the 500 nm SAD pattern found q/a^*=0.5 for the entire grain). Therefore, the superlattice is locally incommensurate with a highly uniform period.

riod. This interpretation is forced by the failure of the CBED probe to record in any sampling the wave number q/a^* =0.5 that would correspond to (orbitally ordered) alternating (200) planes[3] of Mn^{3+} and Mn^{4+} (we use these labels for convenience even though extreme charge separation is not expected[20]). This failure to observe these alternating planes is surprising in the traditional CO picture because at x =0.52, they should predominate, with the alternating pattern broken only by a few extra Mn^{4+} planes for charge neutrality. These extra Mn^{4+} planes would render the superlattice period $(2\pi/q)$ nonuniform and are expected[17,18] on average every 9.6 nm [assuming[4,23] a fine random mixture of two CO phase subunit species with $q/a^*=\frac{1}{2}$ and $\frac{2}{3}$] or 6.8 nm [assuming[18] that the subunits are (002) planes of either Mn^{3+} or Mn^{4+}]. Our 3.6 nm CBED probe is therefore small enough to look between the putative extra Mn^{4+} planes (but large enough to sample a few superlattice periods). In the CO picture, CBED should thus record q/a^*=0.5 in most measurements. However, in ten separate grains where q/a^*<0.5 globally, our CBED probe never found q/a^*=0.5. A typical CBED pattern appears in Fig. 1(b). (Note that an 11th grain had q/a^* =0.5 globally. This possibility was previously highlighted,[24] but the present work shows that it is not a representative scenario.)

Figure 2 reveals that the orientation of the $Pr_{0.48}Ca_{0.52}MnO_3$ superlattice varies in space. We could not clearly resolve this in Fig. 1 because of averaging [Fig. 1(a)] and large-diameter reflections [Fig. 1(b)], but it is readily apparent (**q** not parallel to **a***) in a typical 100 nm SAD pattern taken at 90 K [Fig. 2(b)]. A dark-field image of the region from which this SAD pattern was taken shows variations in superlattice orientation on the nanoscale [Fig. 2(c)]. At higher temperatures, there is no angular variation in 100 nm SAD patterns [180 K, Fig. 2(d)] but, in fact, the nanoscale variations persist [Fig. 2(e)]. Angular variations on any length scale cannot be reconciled with dominant local coupling, in general, or the traditional CO picture,[3–5] in particular, because it is based on (200) planes. Although angular
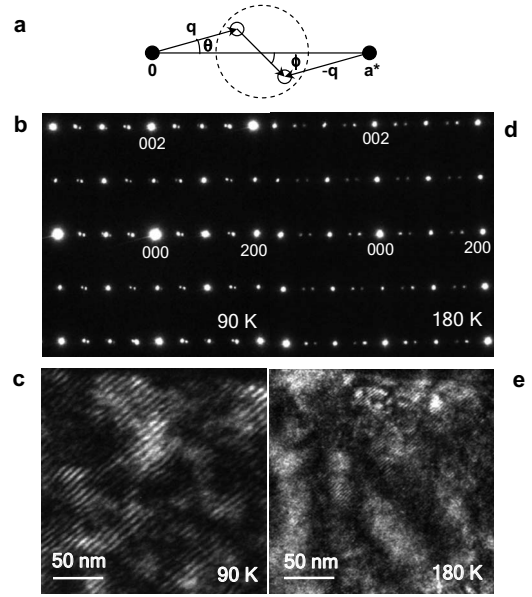

FIG. 2. Local variations in the orientation of the superlattice in the same region of a $Pr_{0.48}Ca_{0.52}MnO_3$ grain. (a) Schematic diffraction pattern showing the relation between parent lattice reflections (●), superlattice reflections (○), and the objective aperture (---). Angles θ and ϕ are exaggerated for clarity. At 90 K, we show (b) a 100 nm SAD pattern and (c) a dark-field image. At 180 K, we show (d) a 100 nm SAD pattern and (e) a dark-field image. From (b), it is apparent that in a spatial average over 100 nm, the superlattice wave vector **q** contains a component along **c*** and is misaligned ($\theta\neq0$) with respect to the parent lattice wave vector **a***. From (d), we see that this misorientation is absent at 180 K. Both dark-field images show interference fringes formed as a consequence of two nearby superlattice reflections (e.g., at **q** and **a***−**q**) falling within the objective aperture and reveal that variations in superlattice misalignment arise on the nanoscale.

variations could, in principle, arise via some complex arrangement of Mn^{3+} and Mn^{4+}, they are most simply interpreted in a scenario where the electron-lattice coupling is limited due to competition with other degrees of freedom.

Figure 3 compares the magnitude q/a^* [Fig. 3(a)] and orientation θ [Fig. 3(b)] of the superlattice wave vector (obtained from 100 nm SAD patterns taken from approximately the same location) with the bulk magnetization M [Fig. 3(c)] measured using a Quantum Design superconducting quantum interference device. Below 150 K, (1) all but one value of θ is nonzero within error and the material is primarily antiferromagnetic,[9,17] and (2) $q/a^*\approx0.46$ varies little with temperature, but falls short of the expected[13] $(1-x)$=0.48 perhaps due to pinning[21] [which would also produce the local variations in superlattice orientation seen in Figs. 2(c) and 2(e)]. Above 150 K, q/a^* develops a strong temperature dependence [Fig. 3(a)], and all but three values of θ are zero within error [Fig. 3(b)]. This transition in θ at 150 K likely represents the Néel transition in the sampled grain (T_N =170 K for $Pr_{0.5}Ca_{0.5}MnO_3$),[9,17] and it is consistent with the onset of the bulk antiferromagnetic transition on warming [Fig. 3(c)]. Given that θ is only nonzero below T_N, we suggest that on a 100 nm measurement length scale, variations in superlattice orientation are intimately linked to the antifer-
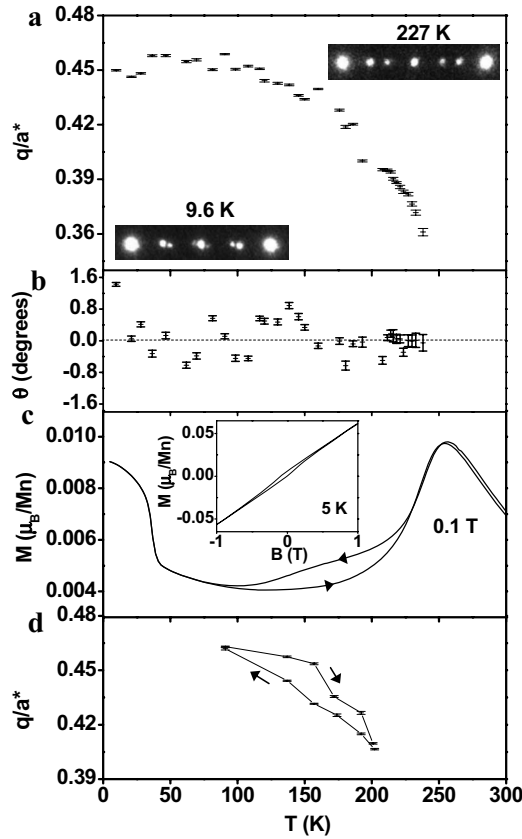
FIG. 3. Temperature dependence of electron diffraction and magnetization data for $Pr_{0.48}Ca_{0.52}MnO_3$. Values of (a) q/a^* and (b) θ obtained from 100 nm SAD patterns taken from approximately the same region within a grain on warming. In (a), we present the 227 and 9.6 K SAD patterns. As seen in (b), we find $\theta \neq 0$ (for all but one measurement) below ~150 K and (in all but three measurements) $\theta = 0$ above ~150 K. In (b), the magnitude of θ should only be interpreted to be zero or finite since the sampled area (i) contains nanoscale variations [Figs. 2(c) and 2(e)] and (ii) is subject to thermal drift. (c) The magnetization M of a bulk sample on cooling and warming in 0.1 T reveals the expected (Ref. 17) antiferromagnetic transition in 100–250 K. Thermal hysteresis is seen in both (c) M and (d) q/a^* obtained from 100 nm SAD patterns taken within a grain on warming and cooling (in a nitrogen stage). The expected (Ref. 10) ferromagnetic component that develops below 40 K shows magnetic hysteresis [inset of (c)], and there is weak evidence for a small concomitant decrease of q/a^*. Error bars in q/a^* and θ indicate the standard deviation of the values extracted from the diffraction pattern.

romagnetic order (see later). We support this argument by noting that (1) M [Fig. 3(c)] and q/a^* [Fig. 3(d)] both show thermal hysteresis in approximately 100 K $< T <$ 200 K; (2) q/a^* in 90 K CBED patterns is reduced by 2% when measured using a Lorentz lens and thus avoiding the 2 T objective field; and (3) below 40 K [Fig. 3(c)], the development of a small ferromagnetic component[10] [inset of Fig. 3(c)] is accompanied by weak evidence for a small reduction in q/a^* [Fig. 3(a)].

It is surprising that in bulk $Pr_{0.48}Ca_{0.52}MnO_3$, we find the superstructure to be (1) locally incommensurate [Fig. 1(b)] and (2) misaligned with the parent lattice [Figs. 2(b), 2(c), 2(e), and 3(b)]. (Pr,Ca)MnO$_3$ has hitherto been
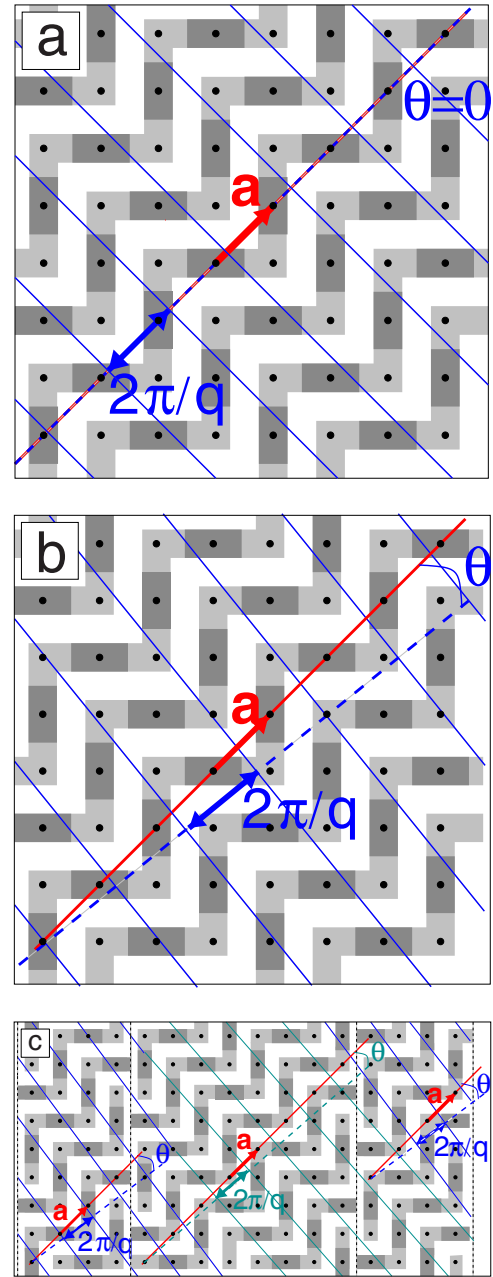

FIG. 4. (Color online) Variations in superlattice misalignment from competition between locally uniform charge modulation and limited local electron-lattice (Jahn-Teller) coupling. Dots represent Mn atoms in this (010) cross section. We assume CE-type antiferromagnetism, where ferromagnetic zig zag chains of Mn (shaded) are antiferromagnetically coupled to neighboring chains, and the valence electron density is larger on the bridge sites (dark) than the corner sites (light). The locally incommensurate superlattice is represented by parallel lines that denote maxima in charge density, and the on-site Jahn-Teller energy saving is maximized when these lines fall as close as possible to bridge sites. Within an antiferromagnetic domain, the charge-density maxima fall out of sync with the bridge sites when the superlattice (wave number q) is (a) collinear or (b) misaligned with respect to the orthorhombic axis **a**. (c) The presence of suitably spaced antiferromagnetic domain walls and variations in θ permits the charge-density maxima of a noncollinear modulation to remain everywhere near the bridge sites.

considered[1,7,9–12] to display the most extreme CO phases of manganites because Pr^{3+} is smaller than La^{3+},[25] because CMR effects are maximized,[7] and because there are no FMM phases at any doping.[10] However, our findings show that the superstructure cannot be interpreted so directly as a manifestation of extreme CO. If the local electron-lattice (Jahn-Teller) coupling does not dominate in as extreme a manganite composition as $(Pr,Ca)MnO_3$, its prominence must be diminished in manganite physics generally.

The magnetic correlations seen in Fig. 3 also require the local electron-lattice coupling to compete with other interactions rather than to dominate. The diffraction patterns in Figs. 2 and 3 suggest that θ is finite below T_N and zero above, and Fig. 3(b) tends to confirm this. It is not known whether the local magnetic order in the antiferromagnetic state is locally commensurate as it might be in the modulated phases of $(La,Ca)MnO_3$,[26] but we assume commensurability, which implies that the coupling is not as weak as we have previously suggested may be possible.[18,19] Figure 4 shows that the Jahn-Teller energy saving may be maximized if spatial variations in θ are associated with the presence of variable-width domains in a CE-type[27] antiferromagnetic configuration. In this cartoon, our typical 100 nm SAD value of $\theta \sim 0.5°$ suggests domains of 22 nm width (1° yields 10 nm). This width is less than our 100 nm measurement length scale and is consistent with the nanoscale variations in θ [Figs. 2(c) and 2(e)] which arise due to the Jahn-Teller coupling [and as seen in Fig. 2(e) persist above T_N]. Note that large local variations in θ would be consistent in our interpretation (Fig. 4) with the presence of domain walls perpendicular to those depicted, as these produce a sign change in θ.

Our demonstration of limited local coupling in manganites is not consistent with the extremely high electrical resistivities that might be expected in the CO picture. However, this expectation has no experimental validity. The modulated phases possess an activated resistivity with a gap of just ~ 0.1 eV, which corresponds to narrow-gap semiconducting behavior.[28,29] Note that the absolute resistivity of $(Pr,Ca)MnO_3$ (10^4 Ω cm at 100 K) (Refs. 22 and 30) is 5–6 orders of magnitude smaller than a good ferroelectric[31] which renders invalid the possibility[32] of ferroelectric measurements. In practice, measurements of resistance may yield significant overestimates of resistivity due to twins which are typically present even in single crystals.[33]

The "electronically soft" reinterpretation[13] of manganites may be understood in the context of our surprise demonstration that the local electron-lattice coupling in manganites is not excessive. It remains a possibility that the local coupling is sufficiently weak[13,18–20] for the modulated phases of manganites to be best described in a charge-density wave scenario[18] rather than in the traditional CO interpretation. Indeed, some degree of electron itinerancy is consistent with the reported resistivity data discussed above. Therefore, the nature of the superlattice remains an open question.

*ndm12@cam.ac.uk

[1] E. Dagotto, *Nanoscale Phase Separation and Colossal Magnetoresistance* (Springer, Berlin, 2002).

[2] C. Israel, M. Calderón, and N. D. Mathur, Mater. Today **10**, 24 (2007).

[3] C. H. Chen and S.-W. Cheong, Phys. Rev. Lett. **76**, 4042 (1996).

[4] S. Mori, C. H. Chen, and S.-W. Cheong, Nature (London) **392**, 473 (1998).

[5] J. B. Goodenough, Phys. Rev. **100**, 564 (1955).

[6] S. Jin et al., Science **264**, 413 (1994).

[7] A. Anane et al., Phys. Rev. B **59**, 77 (1999).

[8] Y. A. Soh et al., J. Appl. Phys. **91**, 7742 (2002).

[9] Z. Jirák et al., J. Magn. Magn. Mater. **53**, 153 (1985).

[10] C. Martin, A. Maignan, M. Hervieu, and B. Raveau, Phys. Rev. B **60**, 12191 (1999).

[11] C. N. R. Rao and P. V. Vanitha, Curr. Opin. Solid State Mater. Sci. **6**, 97 (2002).

[12] R. J. Goff and J. P. Attfield, Phys. Rev. B **70**, 140404 (2004).

[13] G. C. Milward, M. J. Calderón, and P. B. Littlewood, Nature (London) **433**, 607 (2005).

[14] H. Y. Hwang, S.-W. Cheong, N. P. Ong, and B. Batlogg, Phys. Rev. Lett. **77**, 2041 (1996).

[15] P. Schiffer, A. P. Ramirez, W. Bao, and S.-W. Cheong, Phys. Rev. Lett. **75**, 3336 (1995).

[16] P. G. Radaelli, D. E. Cox, M. Marezio, and S.-W. Cheong, Phys. Rev. B **55**, 3015 (1997).

[17] Z. Jirák et al., Phys. Rev. B **61**, 1181 (2000).

[18] J. C. Loudon et al., Phys. Rev. Lett. **94**, 097202 (2005).

[19] S. Cox et al., Phys. Rev. B **73**, 132401 (2006).

[20] L. Brey, Phys. Rev. Lett. **92**, 127202 (2004).

[21] J. C. Loudon, D. E. Cox, N. D. Mathur, and P. A. Midgley, Philos. Mag. **85**, 999 (2005).

[22] R. K. Zheng et al., Phys. Rev. B **70**, 014408 (2004).

[23] C. H. Chen, S. Mori, and S.-W. Cheong, J. Phys. IV **9**, Pr10 (1999).

[24] S. Cox et al., arXiv:0704.2598 (unpublished).

[25] R. D. Shannon, Acta Crystallogr., Sect. A: Cryst. Phys., Diffr., Theor. Gen. Crystallogr. **32**, 751 (1976).

[26] M. Pissas and G. Kallias, Phys. Rev. B **68**, 134414 (2003).

[27] E. O. Wollan and W. C. Koehler, Phys. Rev. **100**, 545 (1955).

[28] C. Cui and T. A. Tyson, Appl. Phys. Lett. **83**, 2856 (2003).

[29] M. R. Lees et al., J. Phys.: Condens. Matter **8**, 2967 (1996).

[30] C. Martin et al., J. Magn. Magn. Mater. **202**, 11 (1999).

[31] R. Waser and M. Klee, Integr. Ferroelectr. **2**, 23 (1992).

[32] D. V. Efremov, J. van den Brink, and D. I. Khomskii, Nat. Mater. **3**, 853 (2004).

[33] R. Wang, J. Gui, Y. Zhu, and A. R. Moodenbaugh, Phys. Rev. B **63**, 144106 (2001).